Article

Molecular Cell

Mitochondrial Protein Interaction Mapping Identifies Regulators of Respiratory Chain Function

Graphical Abstract

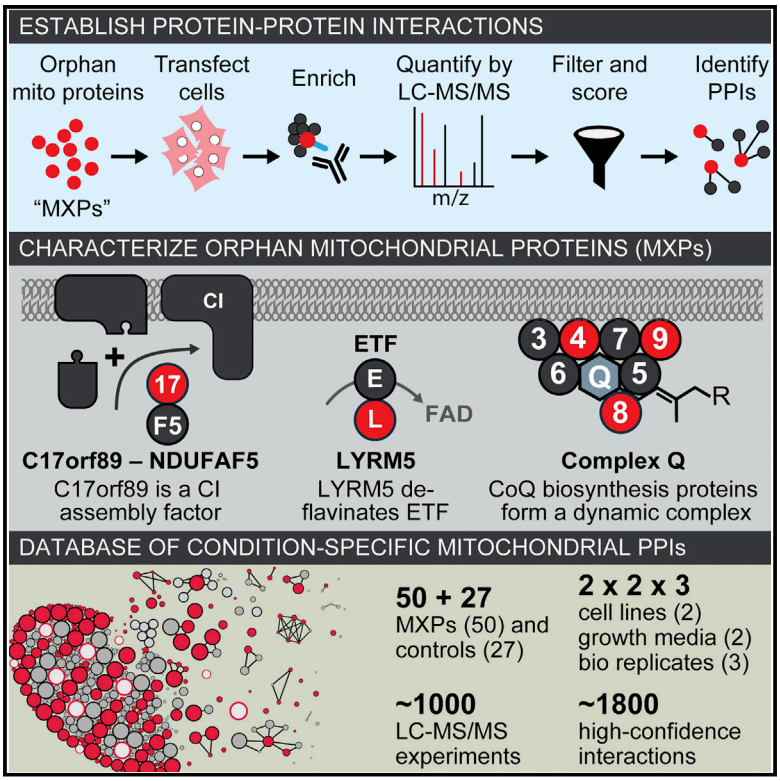

Highlights

- PPI mapping of 50 MXPs reveals mitochondrial protein functions
- C17orf89 is a CI assembly factor depleted in a case of CI deficiency
- LYRM5 interacts with and deflavinates the electron transferring flavoprotein
- Proteins involved in coenzyme Q biosynthesis form a dynamic "complex Q"

Authors

Brendan J. Floyd, Emily M. Wilkerson, Mike T. Veling, ..., Jung-Ja P. Kim, Joshua J. Coon, David J. Pagliarini

Correspondence

dpagliarini@morgridge.org

In Brief

Mitochondria are essential organelles, yet hundreds of their proteins lack robust functional characterization. Floyd et al. (2016) define interaction partners for 50 such proteins, providing hypotheses about their roles in mitochondria. In particular, their work lends mechanistic insight into respiratory chain activities related to complex I, the electron transferring flavoprotein, and coenzyme Q.

Floyd et al., 2016, Molecular Cell 63, 1–12
August 18, 2016
http://dx.doi.org/10.1016/j.molcel.2016.06.033

CellPress

Please cite this article in press as: Floyd et al., Mitochondrial Protein Interaction Mapping Identifies Regulators of Respiratory Chain Function, Molecular Cell (2016), http://dx.doi.org/10.1016/j.molcel.2016.06.033

Molecular Cell
Article

Mitochondrial Protein Interaction Mapping Identifies Regulators of Respiratory Chain Function

Brendan J. Floyd,[1,2,10] Emily M. Wilkerson,[3,10] Mike T. Veling,[1,2,10] Catie E. Minogue,[3,10] Chuanwu Xia,[4] Emily T. Beebe,[2] Russell L. Wrobel,[2] Holly Cho,[1,2] Laura S. Kremer,[5,6] Charlotte L. Alston,[7] Katarzyna A. Gromek,[2] Brendan K. Dolan,[2] Arne Ulbrich,[3] Jonathan A. Stefely,[1,2] Sarah L. Bohl,[1,2] Kelly M. Werner,[2] Adam Jochem,[1] Michael S. Westphall,[9] Jarred W. Rensvold,[1] Robert W. Taylor,[7] Holger Prokisch,[5,6] Jung-Ja P. Kim,[4] Joshua J. Coon,[3,8,9] and David J. Pagliarini[1,2,*]

[1]Morgridge Institute for Research, Madison, WI 53715, USA
[2]Department of Biochemistry
[3]Department of Chemistry
University of Wisconsin–Madison, Madison, WI 53706, USA
[4]Department of Biochemistry, Medical College of Wisconsin, Milwaukee, WI 53226, USA
[5]Institute of Human Genetics, Technische Universität München, 81675 München, Germany
[6]Institute of Human Genetics, Helmholtz Zentrum München, 85764 Neuherberg, Germany
[7]Wellcome Trust Centre for Mitochondrial Research, Institute of Neuroscience, The Medical School, Newcastle University, Newcastle upon Tyne NE2 4HH, UK
[8]Department of Biomolecular Chemistry
[9]Genome Center of Wisconsin
University of Wisconsin–Madison, Madison, WI 53706, USA
[10]Co-first author
*Correspondence: dpagliarini@morgridge.org
http://dx.doi.org/10.1016/j.molcel.2016.06.033

SUMMARY

Mitochondria are essential for numerous cellular processes, yet hundreds of their proteins lack robust functional annotation. To reveal functions for these proteins (termed MXPs), we assessed condition-specific protein-protein interactions for 50 select MXPs using affinity enrichment mass spectrometry. Our data connect MXPs to diverse mitochondrial processes, including multiple aspects of respiratory chain function. Building upon these observations, we validated C17orf89 as a complex I (CI) assembly factor. Disruption of C17orf89 markedly reduced CI activity, and its depletion is found in an unresolved case of CI deficiency. We likewise discovered that LYRM5 interacts with and deflavinates the electron-transferring flavoprotein that shuttles electrons to coenzyme Q (CoQ). Finally, we identified a dynamic human CoQ biosynthetic complex involving multiple MXPs whose topology we map using purified components. Collectively, our data lend mechanistic insight into respiratory chain-related activities and prioritize hundreds of additional interactions for further exploration of mitochondrial protein function.

INTRODUCTION

Mitochondria are centers of metabolism for nearly all eukaryotic cells. Once considered to be mere sites of ATP generation, it is now appreciated that mitochondria participate in a wide range of essential functions related to cellular metabolism, signaling, and programmed cell death (Pagliarini and Rutter, 2013). Consistently, large-scale proteomics- and computation-based efforts during the past decade have revealed that the mitochondrial proteome is much more extensive than once thought, and dysfunction of these organelles is now associated with hundreds of inborn errors of metabolism and common diseases (Koopman et al., 2012; Nunnari and Suomalainen, 2012).

Despite our advanced cataloging of the mammalian mitochondrial proteome, functional characterization of these proteins is far from complete (Calvo et al., 2016; Pagliarini et al., 2008). This gap in knowledge has limited our understanding of basic mitochondrial biology and has obscured the nature and cause of many mitochondrial diseases. For instance, many patients with biochemically established mitochondrial diseases lack mutations in known mitochondrial disease genes, implying the existence of unidentified proteins whose proper functions are necessary for the affected processes (Calvo et al., 2010; Haack et al., 2011). Alternatively, other diseases arise from mutations in mitochondrial proteins with no known functions, making it difficult to interrogate the molecular mechanisms of the diseases.

Protein-protein interactions (PPIs) can provide powerful insight into protein function. Recent advancements in affinity enrichment mass spectrometry (AE-MS) (Hein et al., 2015;

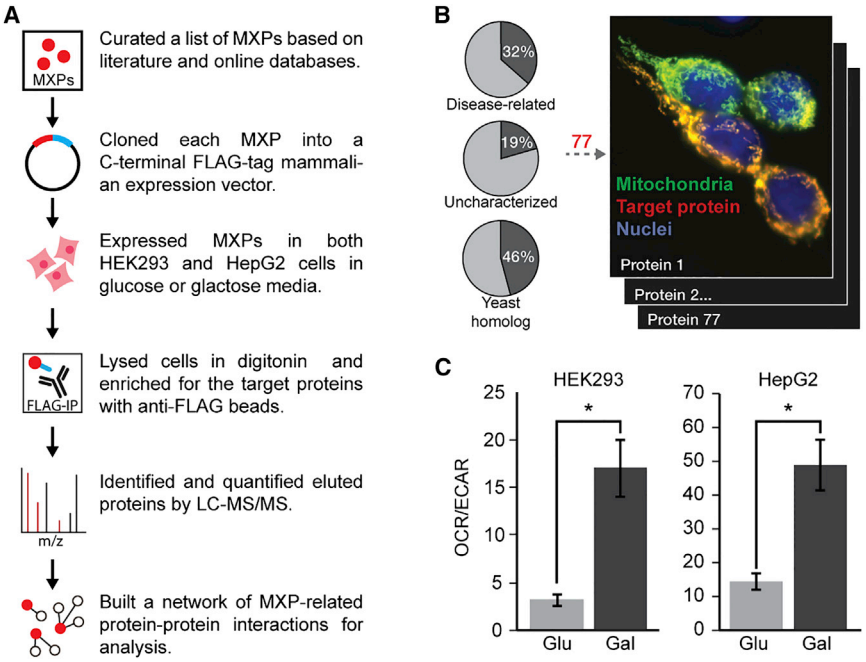

Figure 1. AE-MS Methodology

(A) Schematic workflow of the AE-MS method.

(B) Localization of all FLAG-tagged constructs was established based on MLS-GFP and anti-FLAG fluorescence microscopy (see Figure S1). Venn diagrams report the percentage of the MitoCarta+ list (Table S1) associated with each category.

(C) Galactose induces mitochondrial respiration. Ratio of rates of oxygen consumption (OCR) and extracellular acidification (ECAR) in HEK293 (left) and HepG2 (right) cells grown in 10 mM glucose (Glu) or galactose (Gal) for 24 hr prior to assay. OCR/ECAR is proportional to mitochondrial versus glycolytic flux (asterisk indicates t test $p < 0.05$). Error bars indicate ± SEM.

RESULTS

At Least 20% of the Mitochondrial Proteome Lacks Functional Annotation

Previous analyses have suggested that much of the mitochondrial proteome is uncharacterized (Pagliarini et al., 2008; Pagliarini and Rutter, 2013). To capture an up-to-date assessment of mitochondrial proteins and their functions, we combined the recently updated MitoCarta 2.0 list (Calvo et al., 2016) with additional literature sources to generate a MitoCarta+ list of 1,166 human proteins with validated mitochondrial localization (see Table S1 available online). Next, we annotated these proteins based on the integration of online databases and analysis of the current literature (see Experimental Procedures). Our data indicate that at least 228 mitochondrial proteins have no known, or poorly established, biochemical function, and that an additional 26 proteins with dual localization to the mitochondrion and another cellular compartment do not have clear roles within the mitochondrion. These MXPs constitute ~20% of the mammalian mitochondrial proteome and include many proteins associated with human disease (Table S1; Supplemental Experimental Procedures).

Overall Experimental Strategy

To begin characterizing the functions of MXPs, we elected to establish MXP-specific interactions via AE-MS—an approach proven to be capable of efficiently connecting uncharacterized proteins to known pathways (Figure 1A). We prioritized an initial set of 50 MXPs (Table S1) based on disease relevance, evolutionary conservation, and confirmed localization to mitochondria when possessing a C-terminal FLAG-tag (Figures 1B and S1). We supplemented these bait proteins with 27 mitochondrial proteins of known function (Table S1) and a variant of green fluorescent protein harboring an N-terminal mitochondrial localization sequence (MLS-GFP-FLAG). We performed our interaction analyses in two cell lines (HEK293 and HepG2) grown in both glucose- and galactose-based media conditions. Galactose is known to increase oxygen consumption and dependence on mitochondrial respiratory chain function, which we observed in both lines (Figure 1C). We collected three replicates (i.e., distinct

Hosp et al., 2015; Huttlin et al., 2015; Keilhauer et al., 2015) have improved the ability to accurately detect PPIs, enabling researchers to overcome the systematic bias against poorly characterized proteins inherent in many large-scale "interactome" analyses (Sahni et al., 2015). With AE-MS, a protein of interest (i.e., the bait) is enriched from a sample; it and any co-enriching proteins are then analyzed by mass spectrometry (MS). In this process, the majority of captured proteins are typically not meaningful interactors of the bait. To sort the so-called wheat from the chaff, the AE-MS approach combines the analyses of multiple baits with a robust quantitative MS platform and a scoring algorithm to differentiate between informative interactions and nonspecific background co-enrichment.

In this study, we began by curating a list of proteins from the mitochondrial proteome that lack significant functional annotation, which we call *m*itochondrial uncharacterized (*x*) *p*roteins (MXPs). Using stringent criteria, we conservatively estimate there to be 228 MXPs in humans, including more than 25 that have been associated with human diseases. We then designed a robust AE-MS strategy to define an extensive cell type- and condition-specific interactome of 50 select MXPs, enabling us to propose functions and disease associations for these uncharacterized proteins.

Informed by our large-scale AE-MS analyses, we conducted extensive in vitro biochemistry and cell biology experiments that validated roles for MXPs in various aspects of the mitochondrial respiratory chain. We establish C17orf89 as a complex I (CI) assembly factor, whose silencing markedly impairs CI activity, and whose depletion is found in an unresolved case of isolated CI deficiency. We also establish LYRM5 as a "deflavinase" that directly regulates the electron transferring flavoprotein (ETF) and identify a dynamic human coenzyme Q biosynthetic complex that includes multiple MXPs. We propose functions for a variety of other MXPs and make our data freely available to the community to accelerate further annotation of mitochondrial proteins.

cell transfections) of each condition for a total of 12 analyses per bait protein.

Following anti-FLAG immunoaffinity enrichment, protein eluate was analyzed using nanoflow liquid chromatography coupled to high-resolution MS (quadrupole linear ion trap-Orbitrap hybrid, nLC-MS/MS). Analysis of these 78 unique baits required 936 nLC-MS/MS experiments that generated 20 million MS/MS spectra, identified 5 million unique peptides, and resulted in the observation of 10,000 unique proteins. On average, each nLC-MS/MS experiment detected ~1,000 unique proteins; however, each bait likely has far fewer bona fide interactions. To help distinguish genuine interactions from background, we utilized CompPASS, a known and validated algorithmic approach for highlighting high-confidence interactions and removing non-specific binders (Sowa et al., 2009), modified to incorporate label-free quantitation data.

AE-MS Analyses Identify Hundreds of Mitochondrial Protein Interactions

To assess the performance of our approach and to determine an appropriate cutoff score, we focused on our positive-control bait proteins that have known binding partners. We curated a list of literature-established PPIs involving our positive-control baits and compared their CompPASS scores to those for all mitochondrial preys (Table S2). We selected a stringent cutoff score that achieved 93% sensitivity for known PPIs while simultaneously eliminating 95% of all observed, likely background, interactions (Figure 2A).

Applying this threshold to the rest of our data, and filtering for proteins in our MitoCarta+ list, we identified 1,829 interactions from a total observed set of 109,817 (Figure 2B; Table S3). Consistent with previous efforts (Jäger et al., 2012), we found that using more than one cell type is an effective means for identifying and prioritizing interactions, as only 32% of interactions are shared between the cell lines when limited to our stringent cutoff score (Figure 2C). Changing the carbon source (i.e., glucose versus galactose) had a more modest effect, with 61% of interactions shared between conditions at our threshold cutoff (Figures 2D and S2); however, the abundances of hundreds of these shared interactions are modulated by these changing conditions (Figure 2E), suggesting that mitochondrial metabolism may be linked to the regulation of PPIs. Thus, our experimental design expanded our search space, enabled the identification of meaningful interactions by excluding nonspecific background, and detected interactions affected by nutrient state.

C17orf89 Is a CI Assembly Factor

We designed our study with an awareness that many known mitochondrial pathways and processes are "missing" enzymes or functional components that could be completed by our MXPs. For example, 45%–60% of biochemically validated cases of CI (Calvo et al., 2010; Haack et al., 2011), CII (Jain-Ghai et al., 2013), and CIII deficiency (Fernández-Vizarra and Zeviani, 2015) lack molecular diagnoses. As such, we prioritized MXPs that interacted with respiratory chain components for functional investigations.

A particularly noteworthy MXP in this category was C17orf89, a 7 kDa protein that interacted with the known CI assembly factor (CIAF) NDUFAF5 (Figure 3A). Out of 1,415 observed preys for C17orf89, 31 mitochondrial proteins were above our cutoff score, and only four interactions were observed in both cell lines. Of these, the highest-scoring interaction was between C17orf89 and NDUFAF5. Reciprocally, only three mitochondrial preys interacted with NDUFAF5 in both cell lines, one of which was C17orf89. We validated this C17orf89-NDUFAF5 interaction by showing that immunoprecipitation of FLAG-tagged C17orf89 from HEK293 cells captured endogenous NDUFAF5 (Figure 3B).

To test the hypothesis that C17orf89 is necessary for CI activity, we used RNAi to knock down (KD) *C17orf89* expression in HEK293 cells via lentiviral shRNA constructs. Indeed, we found that silencing of *C17orf89* had a dramatic effect on CI activity (Figure 3C) and subunit levels (Figure S3A), with no consistent change in the abundance of subunits of other respiratory chain complexes. We also observed a slight decrease in the abundance of a subunit of CIV (Figure S3A) and of CIV activity (Figure S3B), consistent with a recent study suggesting that loss of NDUFAF5 also perturbs CIV (Saada et al., 2012). We further observed a dramatic reduction in the oxygen consumption rates of live *C17orf89* KD cells, both basally and upon stimulation with the uncoupler FCCP (Figure 3D), without change to the extracellular acidification rate (ECAR, a measure of glycolytic activity) (Figure S3C). Notably, transfection of *C17orf89-FLAG*, but not *GFP-FLAG*, into KD cell lines was able to rescue much of the lost CI activity (Figure 3E).

To further assess the functional relationship between C17orf89 and NDUFAF5, we established siRNA-mediated HEK293 KD of *C17orf89*, *NDUFAF4*, *NDUFAF5*, *NDUFAF6*, and the CI subunit *NDUFS3* (Figures S4A–S4E) and analyzed each using MS. Silencing of the target genes resulted in an overall decrease in CI subunits; however, the pattern of subunit changes for the *C17orf89* kd cells was most similar to that of *NDUFAF5* (Figure S4F), further strengthening the C17orf89-NDUFAF5 functional relationship. Strikingly, silencing of *C17orf89*, but not other CIAFs or *NDUFS3*, resulted in a drastic loss of NDUFAF5 protein (Figure 4A), suggesting that the role of C17orf89 in CI assembly likely involves the direct stabilization of NDUFAF5.

Our implication of C17orf89 as a CI assembly factor motivated us to investigate the possibility that its disruption might contribute to unresolved patient cases of isolated CI deficiency. We sequenced *C17orf89* in 125 such cases but did not identify likely pathogenic variants. However, RNaseq analysis on 96 cell lines from mitochondrial disease patients that had previously been analyzed by whole-exome sequencing revealed one case that exhibited an 80% reduction of *C17orf89* reads (Figure 4B). This patient, now 26 years of age, was born to unrelated parents and presented in childhood with acute encephalopathy, seizures, mild spasticity, and neuroradiological features consistent with a diagnosis of Leigh syndrome (bilateral high signal intensities in the basal ganglia and brainstem); a diagnostic muscle biopsy at the age of 14 revealed evidence of an isolated CI defect (<40% control activity; Figure 4C). Respiratory chain activities were normal in the sequenced cultured skin fibroblasts (Figure S4G), as is the case for ~50% of patients exhibiting a respiratory chain defect detected in skeletal muscle, liver, or heart (Kirby et al., 2007), thereby precluding our ability to rescue the defect by reintroduction of wild-type *C17orf89*

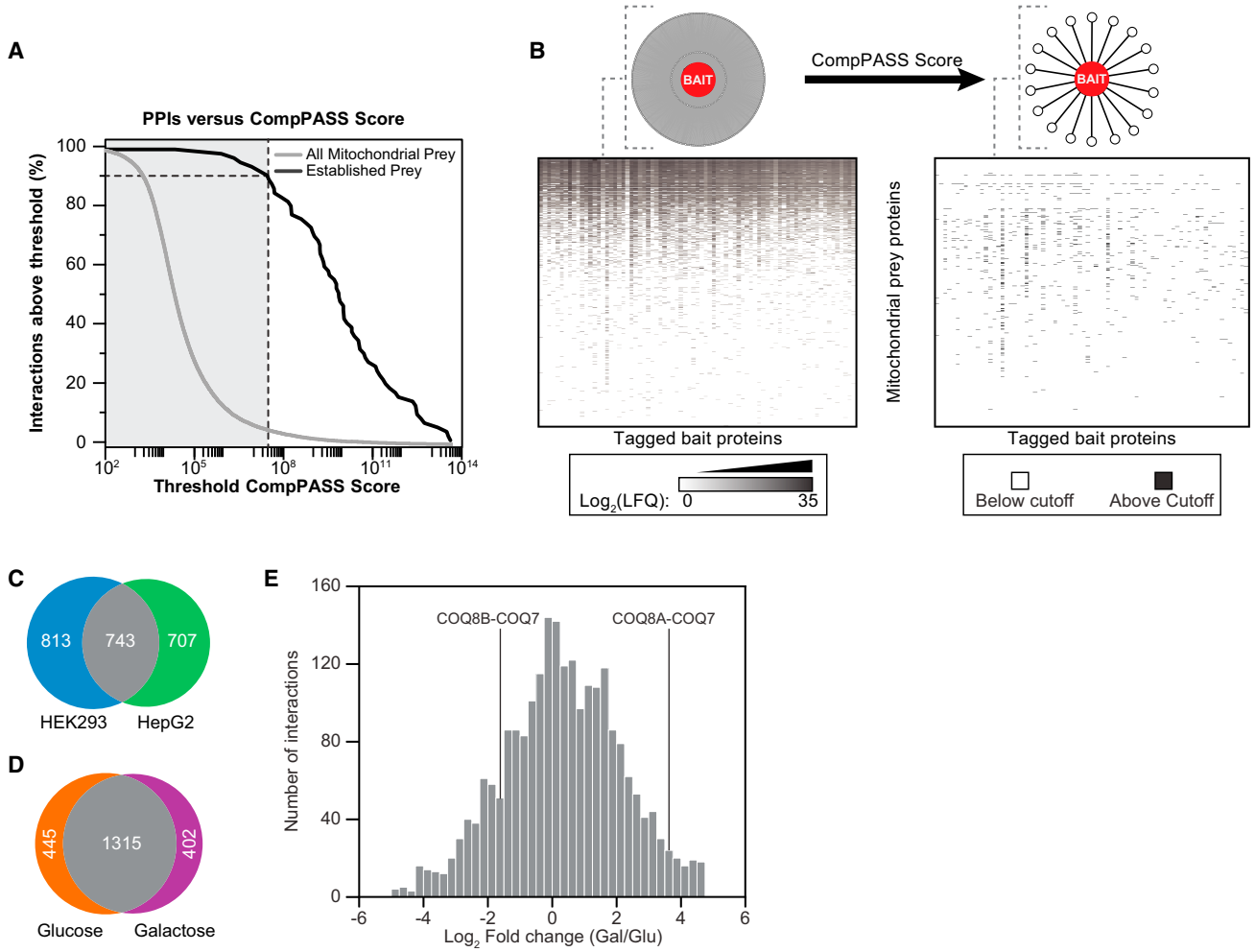

Figure 2. Overall Analyses of Our AE-MS Approach

(A) CompPASS scoring accuracy. CompPASS scores were calculated for all bait-prey interactions, including those involving only mitochondrial prey (gray) and those determined a priori to be high-confidence PPIs based on the literature (black). At each score threshold, the percent of remaining PPI per bin was calculated. Scores to the right of the vertical gray bar exceeded the threshold set for this study and are counted as high-confidence interactions.

(B) Quantitative scoring enriches for high-confidence interactors. (Top) Schematic of the results of CompPASS score filtering. (Bottom left) Heatmap where white indicates a prey was not observed, and shades of gray indicate quantified abundance. Prey proteins are in rows, and FLAG-tagged baits are in columns. Data are averages from six replicates per cell line (three glucose, three galactose). (Bottom right) Heatmap showing scores above CompPASS threshold. Preys and baits are organized in the same order as in left heatmap. Black indicates a score above the threshold. LFQ, label free quantification intensity.

(C) Venn diagram of high-confidence PPIs from each cell line. Mitochondrial interactions above threshold in HEK293 (blue) and HepG2 (green) cells are indicated (see Figure S2).

(D) Venn diagram of high-confidence PPIs from each carbon source. Mitochondrial interactions above threshold in glucose (orange) and galactose (purple) cells are indicated.

(E) Histogram of the fold change abundances of PPIs between carbon sources. Select dynamic PPIs involving proteins from the coenzyme Q biosynthetic pathway (see Figure S6) are indicated.

cDNA. Nonetheless, based on its key role in CI function and its interaction with NDUFAF5 (Figure 4D), we propose to rename *C17orf89* as *NDUFAF8*, and suggest that it is a candidate gene for human CI deficiency.

LYRM5 Binds and Deflavinates the Electron Transferring Flavoprotein

A second MXP that our AE-MS analyses connected to the respiratory chain is LYRM5, an 11 kDa member of the mitochondrial family of LYR motif-containing (LYRM) proteins, which also include MXPs LYRM1, LYRM2, and LYRM9. LYRM proteins were first identified as supernumerary subunits of CI (NDUFA6 and NDUFB9) and have recently been found to act as assembly factors for CII (SDHAF1/LYRM8, SDHAF3/ACN9) (Atkinson et al., 2011; Ghezzi et al., 2009; Sánchez et al., 2013), CV (FMC1) (Lefebvre-Legendre et al., 2001), and iron-sulfur cluster biosynthetic enzymes (ISD11/LYRM4) (Adam et al., 2006; Shan et al., 2007). Our data capture many of these expected LYRM interactions (Figure 5A). Interestingly, all seven LYRM proteins in our study were found to interact with NDUFAB1, a poorly characterized

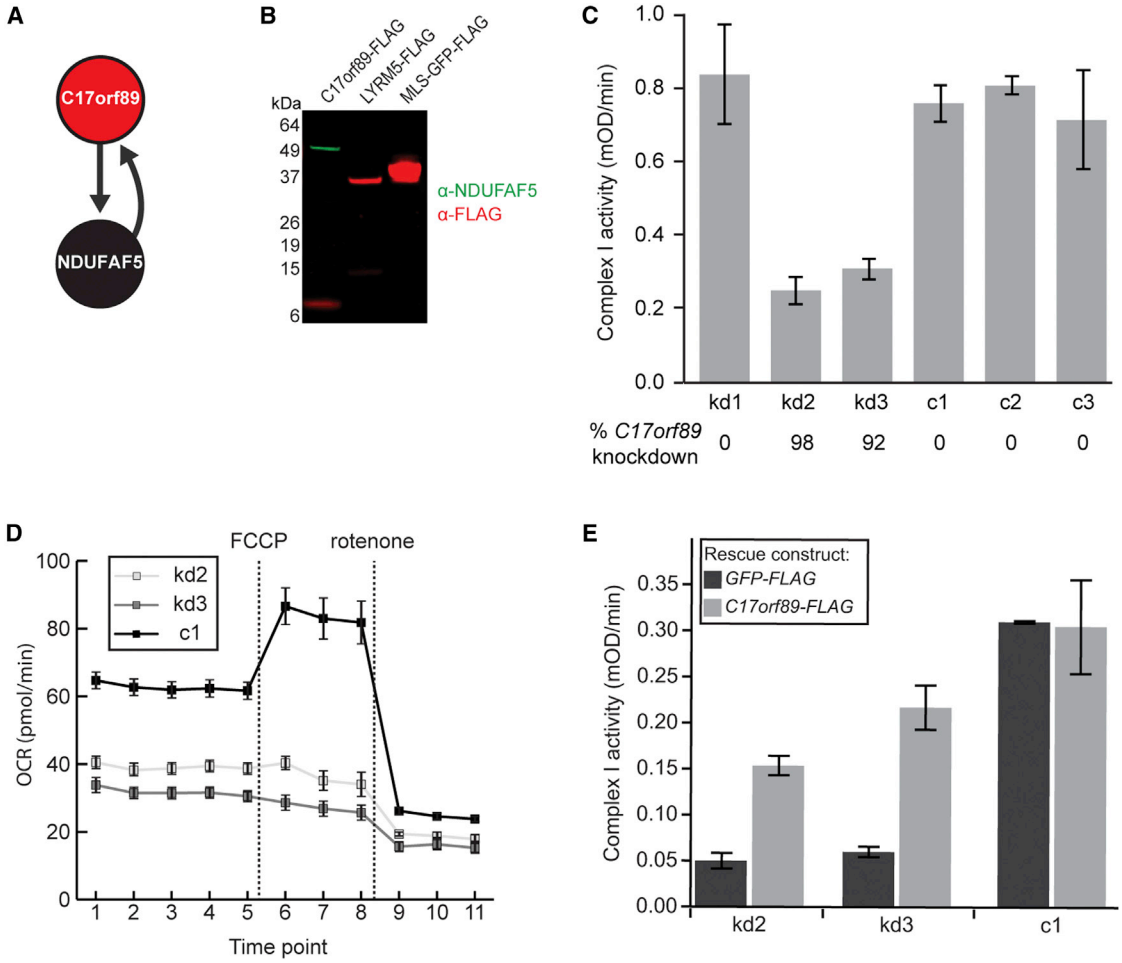

Figure 3. C17orf89 Is Required for Complex I Assembly

(A) Schematic of top-scoring C17orf89 interactions. Arrows originate from bait proteins and point to high-confidence interactors.

(B) Immunoblot of immunoprecipitated FLAG-tagged C17orf89, LYRM5, and MLS-GFP with anti-FLAG (red) or anti-NDUFAF5 (green).

(C) Activity of complex I in *C17orf89* knockdown (kd) and control (c) HEK293 cell lines and control lines. Error bars indicate ± SD (see also Figure S3). Percent reduction in C17orf89 mRNA is indicated for each cell line.

(D) Measurement of oxygen consumption rate (OCR) for the same kd or c lines as in (C) using a Seahorse Extracellular Flux Analyzer (FCCP, carbonyl cyanide *p*-trifluoromethoxyphenylhydrazone). Error bars indicate ± SEM.

(E) Complex I activity in kd and c cell lines after transfection with *GFP-FLAG* (negative control) or *C17orf89-FLAG* (rescue). Error bars indicate ± SD.

CI subunit that also serves as an acyl carrier protein (Angerer et al., 2014) (Figure 5A).

Unlike the other LYRM proteins, LYRM5 interacted robustly with ETFA and ETFB, which comprise the electron transfer flavoprotein (ETF) (Figure 5A). ETF partners with ETF dehydrogenase to shuttle electrons to CoQ. Notably, LYRM5-FLAG immunoprecipitation enriched for endogenous ETFA and ETFB to a much greater extent than does IVD—a known ETF substrate (Kim and Miura, 2004) (Figures 5B and S5). Furthermore, the LYRM5 IP elution generated a single band containing LYRM5, ETFA, and ETFB on a BN-PAGE immunoblot (Figure 5C). To test whether the LYRM5-ETF interaction is direct, we purified recombinant ETF and LYRM5 from *E. coli* (Figure 5D) and demonstrated that they form a stable complex by size-exclusion chromatography (Figure 5E). LYRM5 alone eluted as a broad peak around 44 kDa, indicating that it may exist as a tetramer.

Surprisingly, the purified LYRM5-ETF complex lacked the characteristic yellow color of flavoproteins, suggesting that LYRM5 either prevents the incorporation of flavin adenine dinucleotide (FAD) into ETF or that it is capable of removing this cofactor. To test the ability of LYRM5 to "deflavinate" the ETF complex, we mixed LYRM5 and ETF at increasing ratios and measured ETF activity. The addition of LYRM5 led to a linear reduction of ETF activity up to a ratio of 4:1, at which point ETF lost all activity (Figure 6A). This decrease in activity was concomitant with a proportional release of FAD from the ETF complex, as observed by fluorescence emission spectroscopy (Figure 6B). The interaction of FAD with ETF protein residues can be seen by the 420 nm and 460 nm peaks on an absorbance spectrum. These peaks disappear upon addition of LYRM5 (Figure 6C), lending further evidence of its direct deflavination activity. Collectively, these experiments support a direct, specific

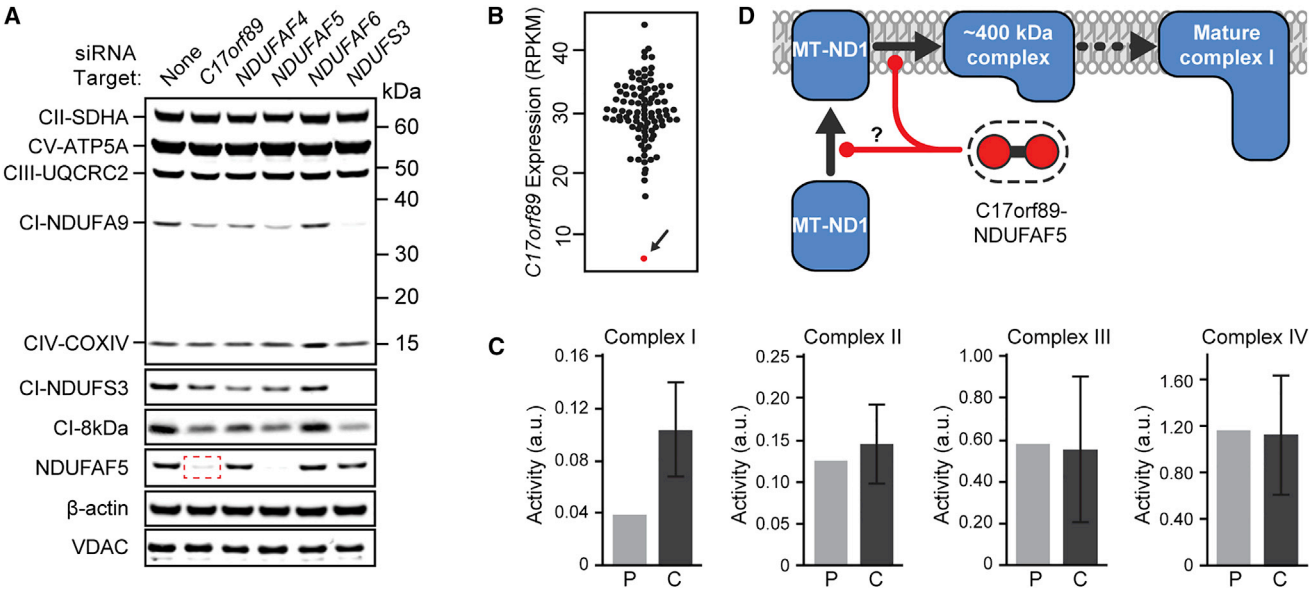

Figure 4. C17orf89 Stabilizes NDUFAF5 and Is Depleted in a Case of CI Deficiency

(A) Immunoblots of mitochondrial proteins in cells treated with siRNA for CI and CIAF genes. *C17orf89* knockdown results in loss of CI subunits and a marked depletion of NDUFAF5 (red box). See also Figure S4.

(B) RNaseq analysis of *C17orf89* expression in 96 cell lines from patients with respiratory chain dysfunction (RPKM, reads per kilobase of transcript per million mapped reads). Arrow indicates a line with severe loss of *C17orf89* expression.

(C) Respiratory chain complex analyses of the patient line indicated in (B), revealing an isolated CI deficiency (P, patient; C, control). Error bars represent mean ± SD, n = 25.

(D) Proposed model of C17orf89–NDUFAF5 complex function in CI assembly.

interaction between LYRM5 and ETF that results in deflavination (Figure 6D)—a unique and unexpected activity that perhaps suggests a non-electron transferring role for ETF (see Discussion).

CoQ Is Synthesized by a Dynamic Biosynthetic Complex

Both CI and ETF operate by shuttling electrons to CoQ—a requisite gateway for electron transport along the mitochondrial respiratory chain. CoQ is synthesized within the mitochondrion in a process that involves at least 13 human proteins, six of which we consider MXPs as they lack well established biochemical roles in the pathway (Figure S6A). Across a series of isolated studies, seven *S. cerevisiae* CoQ proteins, Coq3p–Coq9p, have been found to physically interact and to potentially form a biosynthetic complex (He et al., 2014; Marbois et al., 2005). We and others have speculated that a CoQ complex might exist in other species; however, species-specific aspects of CoQ biosynthesis exist, and, to date, there are only four known human CoQ-related PPIs (Ashraf et al., 2013; Lohman et al., 2014; Nguyen et al., 2014).

Our AE-MS data have now established direct evidence of a highly interconnected mammalian CoQ biosynthetic complex, which we call complex Q (Figure 7A). Intriguingly, the abundances of CoQ pathway PPIs involving COQ8A/ADCK3 increased in galactose-treated cells, and those with COQ8B/ADCK4 reciprocally decreased (Figure 7B)—a phenomenon that accompanied a marked elevation of CoQ levels in HepG2 cells (Figure 7C) (note that ADCK3 and ADCK4 are now referred to as COQ8A and COQ8B, respectively—see Stefely et al. [2016], in this issue of *Molecular Cell*). We consider COQ8A and COQ8B to be MXPs due to their lack of clear biochemical function; however, consistent with these results, we recently revealed that COQ8A is essential for the stability of CoQ proteins in a mouse model of Coq8a deficiency (Stefely et al., 2016), and COQ8B has been shown to interact with COQ6 (Ashraf et al., 2013). These data suggest an important connection between CoQ production and interactions among CoQ biosynthetic complex members and may indicate reciprocal regulation of the activities of the paralogs COQ8A and COQ8B.

We next aimed to reconstruct the CoQ interactions using purified recombinant proteins. This is a powerful means to validate our observed AE-MS interactions, ascertain the direct interactions between the CoQ proteins, and begin mapping the topology of complex Q. Our in vitro analyses using a cell-free protein translation and purification system revealed that while nearly all COQ proteins were unstable or insoluble when produced alone, many coexpression pairs between COQ3–COQ7 and COQ9 were stabilized by direct interaction (Figures 7D, 7E, and S6B). Strikingly, using this same method, we were then able to rebuild a CoQ complex containing six of the core members in vitro (Figures 7G and 7H). Combined with the binary interactions noted above, these data allow us to propose the subunit topology of the complex (Figures 7F and 7H). While it is likely that other CoQ-related proteins interact with the complex directly or indirectly and are important for its stability in vivo, such as COQ8A and COQ8B, this work suggests that these six core CoQ-related proteins are sufficient to form a complex. These data lend clarity to an evolutionarily conserved complex Q and provide a platform

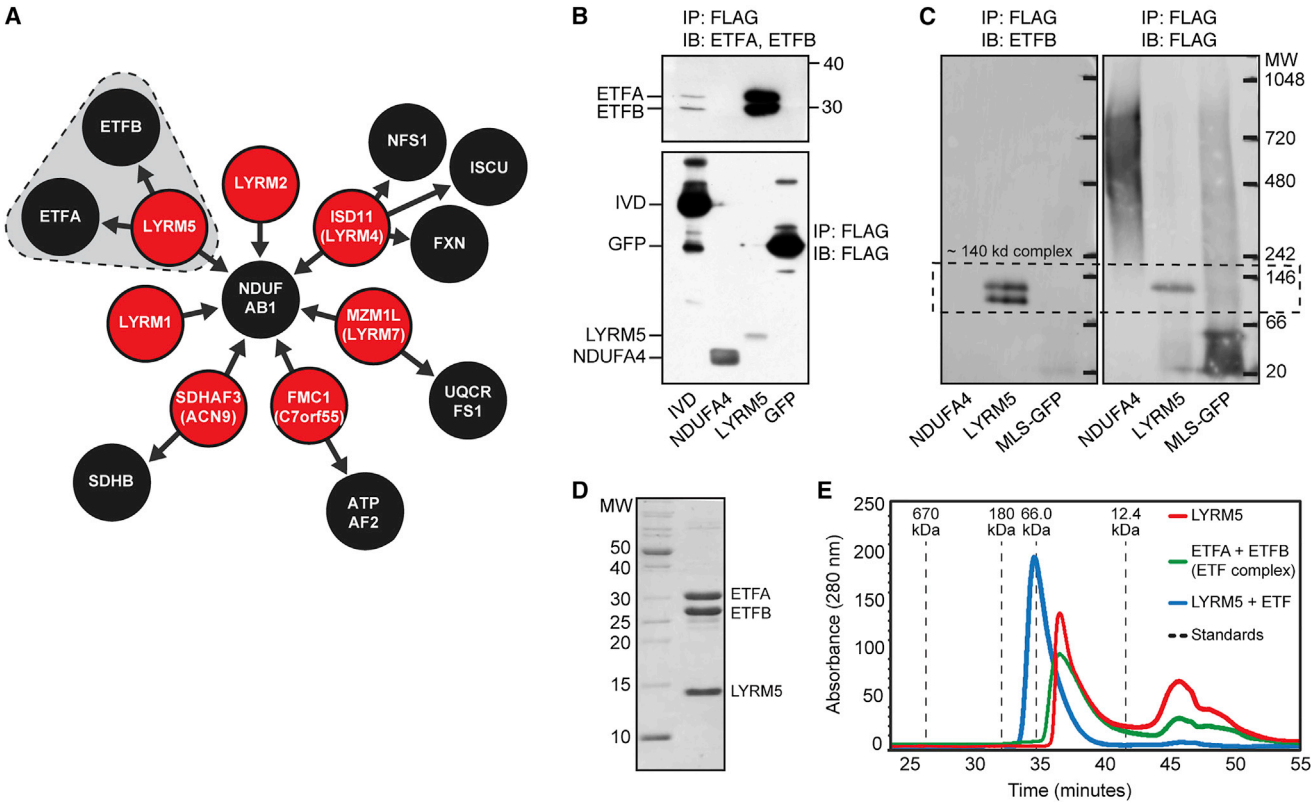

Figure 5. LYRM5 Forms a Complex with ETF

(A) Schematic of top-scoring LYRM PPIs. LYRM5-ETF interactions are shaded.

(B) Validation of the interaction between LYRM5 and both ETFA and ETFB. C-terminally FLAG-tagged GFP, IVD, NDUFA4, and LYRM5 were immunoprecipitated (IP) from HEK cells and immunoblotted (IB) with anti-ETFA and anti-ETFB (upper) or anti-FLAG (lower). LYRM5 enriched for both ETF proteins more efficiently than IVD, a known ETF interactor.

(C) IP of LYRM5-FLAG or MLS-GFP-FLAG from HEK293 cells analyzed by blue native PAGE analysis and IB. The same membrane was blotted for ETFB (left) and then FLAG (right) (see also Figure S5).

(D) Recombinant N-terminally His-tagged LYRM5 and untagged ETFA/B were coexpressed in *E. coli*. Purification of LYRM5 by metal affinity chromatography led to the copurification of ETFA/B.

(E) LYRM5 and ETF form a stable complex. Size-exclusion chromatography of LYRM5 alone (red), ETF alone (green), or the co-purified LYRM5-ETF complex (blue) noted in (D).

for the future interrogation of the roles of each complex subunit, including the MXPs COQ4 and COQ9.

Associating MXPs with Other Established Pathways

Our analyses above focused on MXPs related to CI and CoQ in order to build upon our recent work in these areas (Khadria et al., 2014; Lohman et al., 2014; Stefely et al., 2015). However, our data reveal many other connections between MXPs and diverse mitochondrial processes. For instance, C15orf48 also interacts with multiple subunits of CI and CIV (Figure S7), suggesting that it regulates the activity of one or both of these complexes, or perhaps supercomplex formation. C2orf47 interacts with AFG3L2 and SPG7, the two members of the human m-AAA protease complex that is responsible for the maturation of several membrane-associated proteins and for mitochondrial protein quality processes (Ehses et al., 2009) (Figure S7). As a final example, we observed that DHRS4—a poorly characterized member of the short-chain dehydrogenases/reductases (SDR) family (Persson and Kallberg, 2013)—interacts with other members of the SDR family, including DHRS4L2 and CBR4, as well as with SIRT3 and EHHADH (Figure S7). DHRS4 is reported to have dual localization to peroxisomes and mitochondria (Matsunaga et al., 2008; Pagliarini et al., 2008) and is dynamically phosphorylated and acetylated (Grimsrud et al., 2012; Still et al., 2013); however, no direct function is known. These interactions suggest that DHRS4 might have an important unappreciated role in coordinating lipid metabolism between these organelles. Our other top-scoring interactions, and many others that fall just below our stringent cutoff, can likewise enable new hypotheses about MXP function (Table S2).

DISCUSSION

Insights into Mitochondrial Respiratory Chain Function

Our identification of C17orf89/NDUFAF8 as a complex I assembly factor (CIAF) pinpoints it as a disease gene candidate for

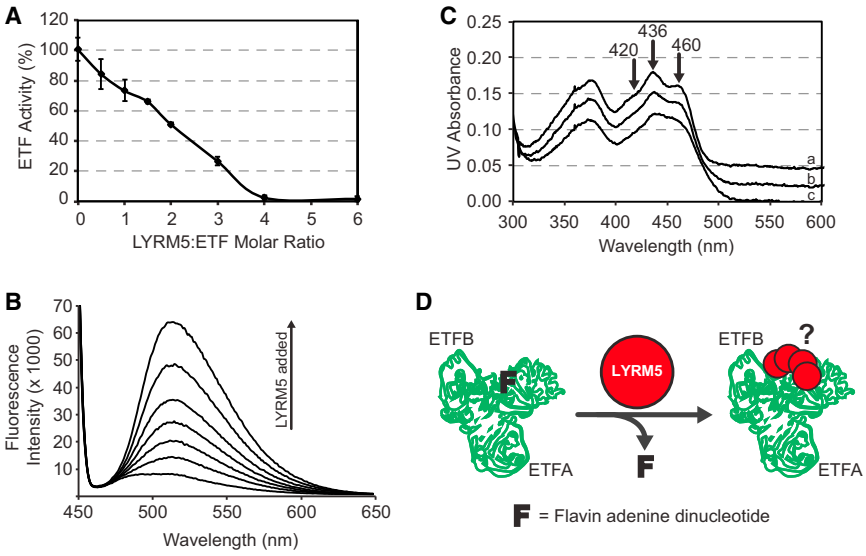

Figure 6. LYRM5 Deflavinates ETF

(A) ETF activity in the presence of increasing amounts of LYRM5 (± SD from triplicate measurements).

(B) FAD release from ETF upon incubation with varying amounts of LYRM5, measured by fluorescence emission spectroscopy.

(C) Visible spectra of ETF in the presence of LYRM5. The flavin visible spectrum shows two shoulder peaks at 420 nm and 460 nm due to the interaction between FAD and ETF protein residues that are lost upon addition of LYRM5. Spectra a, b, and c are for LYRM5:ETF ratios of 0, 2, and 4, respectively. For clarity, spectra a and b have been shifted by +0.04 and 0.02 OD units, respectively.

(D) Proposed model of the functional interaction between LYRM5 and ETF. Binding of four molar equivalents of LYRM5 (red dot) to ETF (green trace of PDB ID 1EFV) leads to the loss of FAD from ETF (F).

unresolved cases of isolated CI deficiency. Given the presence of twin CX_9C domains in its primary structure, C17orf89/NDUFAF8 is likely a member of the coiled-coil-helix-coiled-coil-helix (CHCH) domain family of proteins (Modjtahedi et al., 2016). Many CHCH proteins are mitochondrial, and several are involved in respiratory chain functions, including four CI subunits (Modjtahedi et al., 2016). Our data revealed a robust interaction between C17orf89/NDUFAF8 and NDUFAF5—a putative methyltransferase that is essential for early stages of CI assembly (Pagliarini et al., 2008; Sugiana et al., 2008), but for which neither a substrate nor a direct role in CI maturation has been elucidated. Interestingly, several similar sub-complexes of CIAFs exist, including the mitochondrial CI assembly (MCIA) complex (Guarani et al., 2014) and the NDUFAF3:NDUFAF4 complex (Saada et al., 2009). Given that C17orf89/NDUFAF8 interacts with and stabilizes NDUFAF5, we suggest that C17orf89 may facilitate the methyltransferase activity of NDUFAF5, or even be its substrate. Furthermore, as we identified a patient with CI deficiency whose molecular diagnosis eluded whole-genome sequencing but who is deficient in *C17orf89/NDUFAF8* transcript, we both prioritize this as a disease gene and highlight the importance of complementary methods for the diagnosis of genetic diseases.

CI is one of several sources of electrons entering the CoQ pool for transport along the respiratory chain. A second source is ETF, which interacts with and accepts electrons from various mitochondrial dehydrogenases before passing them to ETFDH (Roberts et al., 1996). ETF harbors causal mutations in glutaric acidemia type 2 (GA2) (Vockley and Whiteman, 2002), and other cases of GA2 remain unresolved (Schiff et al., 2006). Given this, we were particularly interested in our observed interaction of ETF with LYRM5.

We discovered that the interaction between LYRM5 and ETF results in an efficient—and surprising—removal of FAD from the ETF holoenzyme. Much work needs to be done to understand the in vivo utility of this process, but a few possibilities stand out. First, the FAD of ETF could become damaged and need to be replaced. Second, removal of FAD may facilitate the destabilization of ETF and allow for proteolysis and recycling of the flavin cofactor. Third, if in a given metabolic state ETF is not interacting with dehydrogenases (i.e., its electron transfer partners), its FAD would be free to interact with water or other matrix metabolites and generate reactive oxygen species (Rodrigues and Gomes, 2012). In this scenario, LYRM5 could act to shut down ETF activity without the need to completely turn over the enzyme. Finally, it is possible that ETF possesses a distinct, non-electron transferring function—a possibility we most favor. Consistent with this hypothesis is our observation that LYRM5, like other LYRM proteins (Figure 5A), interacts with the CI subunit NDUFAB1—the mitochondrial acyl carrier protein (ACP) (Angerer, 2015; Angerer et al., 2014). It is possible that LYRM5 serves as an adaptor to bring ETF to CI via NDUFAB1 to perform an unidentified function. Given our functional discoveries, we propose renaming *C17orf89* and *LYRM5* as *NDUF Assembly Factor 8* (*NDUFAF8*) and *ETF Regulatory Factor 1* (*ETFRF1*), respectively.

Insights into CoQ Biosynthesis

CoQ is a requisite gateway in the respiratory chain that accepts electrons from many sources, including CI and ETF (via ETFDH). Although it was discovered 60 years ago, multiple aspects of eukaryotic CoQ biosynthesis remain unexplained, including roles for MXPs COQ8A, COQ8B, COQ4, and COQ9 (Figure S6A).

Two notable features emerged from our work with the CoQ machinery. First, it is abundantly clear that the mammalian CoQ proteins physically interact to form what appears to be a biosynthetic complex—complex Q. *Saccharomyces cerevisiae* is also known to have a partially defined complex, but it is not known how this complex facilitates CoQ biosynthesis. Our work here provides insights into the binary interactions that likely enable the formation of complex Q in both species. Second, our work implicates MXPs ADCK3 and ADCK4 (aka COQ8A and COQ8B, respectively) in complex Q and show that their interactions with the complex are both dynamic and reciprocal. COQ8A and COQ8B are paralogs that are each likely orthologs of yeast

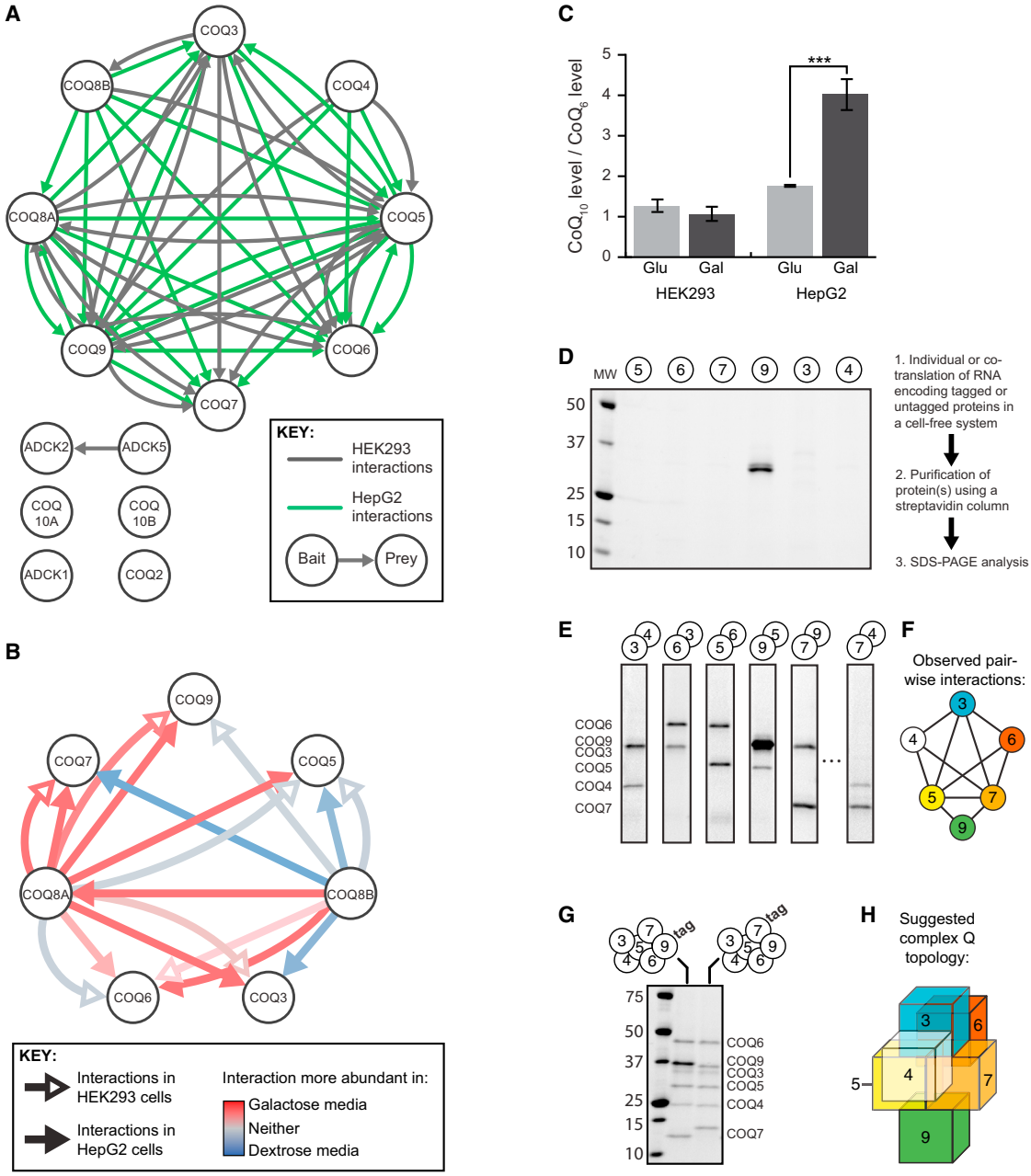

Figure 7. Interaction Analysis Reveals the Dynamic Human CoQ-Related Complex

(A) All CoQ-related proteins used as baits and/or observed as preys in this study are shown as white nodes. Interactions above our score threshold are shown for HEK293 cells (gray arrows) or HepG2 cells (green arrows).

(B) CoQ-related interactions involving COQ8A or COQ8B as bait were assessed for the effect of cellular metabolic status. Interactions more abundant in galactose or glucose media are shown in red or blue, respectively, while those with no clear media effect are in gray. See also Table S3 for primary data.

(C) Relative abundance of CoQ_{10} in HEK293 and HepG2 cells after treatment with 10 mM glucose or galactose for 24 hr (*** indicates t test $p < 0.001$, error bars indicate the 95% confidence interval).

(D and E) Representative results of in vitro protein translation and purification of each core CoQ complex protein individually (D) or in pairs (E). Proteins were run on SDS-PAGE and detected by Coomassie stain. See Figure S6 for all interactions observed.

(F) Schematic of COQ protein network direct interactions established in vitro. All robust interactions are represented as edges between the COQ protein nodes.

(G) In vitro co-purification of all six core COQ complex proteins. "Tag" indicates sole protein with strep tag II affinity tag.

(H) Three-dimensional model of predicted COQ complex structure based on in vitro interaction data. Colors are as in Figure 7F.

Coq8p, and we have speculated that they possess redundant functions in a condition- or tissue-specific manner. We recently have shown that COQ8A adopts an atypical protein kinase-like fold (Stefely et al., 2015) and, building off of the work here, have now determined that its function is essential for maintaining complex Q stability (Stefely et al., 2016).

Overall, we have extended the annotation of the mammalian mitochondrial proteome by identifying robust PPIs involving MXPs and by validating roles for these proteins in well-characterized mitochondrial pathways. Other prominent PPIs from our study now await further biological investigation, and many more that fell below our stringent cutoff score will nonetheless serve as important clues for the functional annotation of MXPs moving forward (Table S3). As such, our compendium of state-specific MXP associations will continue to serve as a powerful resource for the characterization of mitochondrial proteins, thereby advancing our understanding of basic mitochondrial biology and its associated pathophysiology.

EXPERIMENTAL PROCEDURES

Mitochondrial Proteome Compilation

Entrez GeneIDs of the mouse MitoCarta (Pagliarini et al., 2008) were converted from mouse to human using HomoloGene and reciprocal BLASTP searches. Data from the mitochondrial matrix (Rhee et al., 2013), inter-membrane space (Hung et al., 2014) proteomic studies, and other high-quality studies were then integrated with the human MitoCarta 2.0 (Calvo et al., 2016) to generate our MitoCarta+ list of mitochondrial proteins.

Generation of Tagged Constructs

Mitochondrial open reading frames were obtained from The Broad Institute and DNASU (Seiler et al., 2014) and cloned into a pcDNA3.1 mammalian expression vector with a C-terminal FLAG tag.

Mammalian Cell Culture

HEK293 or HepG2 cells were transiently transfected with pcDNA3.1 gene-FLAG plasmids using linear polyethylenimine (PEI, PolySciences) and Opti-MEM (LifeTechnologies). After 48 hr, cells were washed with PBS, and media was replaced with DMEM containing either 10 mM glucose or 10 mM galactose. After 24 hr, cells were washed with and harvested into phosphate-buffered saline (PBS), snap frozen in liquid nitrogen, and stored at −80°C.

Affinity Enrichment

Cell pellets were lysed in 200 μl buffer (see Supplemental Experimental Procedures). After vortexing on ice, insoluble materials were pelleted (16,000 g, 10 min, 4°C). Equal masses of cell supernatant were mixed with 30 μl pre-washed anti-FLAG magnetic beads (Sigma M8823) for 2–3 hr at 4°C with end-over-end agitation. Following incubation, beads were washed four times and proteins were eluted in 70 μl elution buffer containing 0.2 mg/mL FLAG-peptide for 30 min at room temperature with constant agitation.

LC-MS/MS Analysis

All experiments were performed using a NanoAcquity UPLC system (Waters, Milford, MA) coupled to an Orbitrap Elite mass spectrometer (Thermo Fisher Scientific, San Jose, CA). Reverse-phase columns were made in house by packing a fused silica capillary with 3.5 μm diameter, 130 Å pore size Bridged Ethylene Hybrid C18 particles (Waters) to a final length of 30 cm. The column was heated to 55°C for all experiments. Precursor trypsin-digested peptide cations were generated from the eluent through the utilization of a nanoESI source. MS instrument methods consisted of MS^1 survey scans that were used to guide 15 subsequent data-dependent MS/MS scans. Raw data can be found on Chorus (https://chorusproject.org) under project ID 1043.

Data Analysis

Data were processed using the MaxQuant software suite (Cox and Mann, 2008; Cox et al., 2011). Searches were performed against a target-decoy database using the default settings for high-resolution mass spectra. Results were filtered to 1% FDR at the unique peptide level and grouped into proteins within MaxQuant. Proteins were quantified across all replicates within each bait set using MaxLFQ (Cox et al., 2014).

Generation of *C17orf89* Knockdown Cells

Viral particles were produced in HEK293 cells by transient transfection with PEI of lentiviral shRNA construct, psPAX2, and pMD2.G packaging plasmids. HEK293 cells were transduced in 6-well plates and were selected in culture medium supplemented with 2 μg/ml puromycin for at least 2 weeks. For siRNA knockdowns, HEK293 cells were transfected with 10 nM RNA for each target or the non-targeting siRNA based on the manufacturer's protocol. After 2 days, the cells were passaged; the next day were transfected again with 10 nM siRNA; and after another 2 days were collected for real-time qPCR, immunoblot, and MS-based proteomic analyses.

CI Activity and *C17orf89* Sequencing and Expression Analysis

Patients with biochemical evidence of isolated complex I deficiency identified via diagnostic work-up for suspected mitochondrial disease were screened for disruptive variants in *C17orf89* by Sanger sequencing (primers available on request). *C17orf89* transcript abundance in control and patient lines was measured as described previously (Haack et al., 2015). Informed consent for diagnostic and research studies was obtained in accordance with the Declaration of Helsinki protocols and approved by local Institutional Review Boards.

Purification and Functional Analyses of LYRM5 and ETF

LYRM5 was cloned into a pET28a vector and purified as an N-terminally His-tagged protein by immobilized metal affinity chromatography. Size-exclusion chromatography was performed using a Pharmacia 300 × 10 mm Superdex 200 column. ETF activity ± LYRM5 was measured by monitoring DCPIP reduction at 600 nm. For assay conditions, 40 μM DCPIP, 20 μM C_8-CoA, and 0.1∼0.2 μM ETF were mixed in 20 mM Tris-HCl buffer (pH 8.0). The assay reactions were initiated by adding 0.2 μM MCAD, and the UV absorbance decrease at 600 nm was followed for 3 min. FAD release was measured by first mixing 10 μM ETF with varying amounts of LYRM5 and incubated on ice for 2 hr. The samples were then diluted five times in 20 mM Tris-HCl buffer (pH 8.0), and the fluorescence emission spectra were taken at room temperature (λ_{ex} = 436 nm). Visible spectra measurements of 10 μM ETF were measured in the presence of 0, 20, and 40 μM LYRM5 in 20 mM Tris-HCl buffer (pH 8.0).

Blue Native PAGE

Samples were mixed with native PAGE sample buffer to 1× final concentration and were loaded onto native PAGE gels alongside native MARK standard. Gels were run for a total of 2 hr and subsequently subjected to western analysis.

Coenzyme Q Quantification

Tissue culture cells were lysed by vortexing with glass beads and spiked with an internal standard (CoQ_6). Lipids were extracted with $CHCl_3$/MeOH (1:1, v/v) and analyzed by LC-MS/MS.

Cell-free Expression and Purification

Purified plasmid DNA was used as individual transcription templates with SP6 RNase polymerase. Transcription and translation methods are as previously described (Makino et al., 2013).

SUPPLEMENTAL INFORMATION

Supplemental Information includes seven figures, three tables, and Supplemental Experimental Procedures and can be found with this article at http://dx.doi.org/10.1016/j.molcel.2016.06.033.

AUTHOR CONTRIBUTIONS

B.J.F. and D.J.P. conceived of the project and its design. B.J.F, C.E.M., E.M.W., M.T.V., C.X., E.T.B., H.C., L.S.K., C.L.A., K.A.G., B.K.D., A.U., J.A.S., S.L.B., K.M.W., J.W.R., R.W.T., H.P., J.J.K., J.J.C., and D.J.P. performed experiments and data analysis. R.L.W., A.J., M.S.W., J.W.R., R.W.T., H.P., J.J.K., J.J.C., and D.J.P. provided key experimental resources and/or aided in experimental design. B.J.F. and D.J.P. wrote the manuscript.

ACKNOWLEDGMENTS

We thank David Aceti, John Primm, Brian Fox, and John Markley for technical and managerial assistance and Clay Williams for MS technical support. This work was supported by a Searle Scholars Award and NIH grants U01GM94622, R01DK098672, R01GM112057, and R01GM115591 (to D.J.P.); R35GM118110 (to J.J.C.); R01GM029076 (to J.-J.P.K.); T32DK007665 and T32GM008692 MSTP (to B.J.F.); T15LM007359 (to C.E.M.); T32HL007899 (to E.M.W.); F30AG043282 (to J.A.S.); and T32GM07215 (to K.M.W.); and also by a Wisconsin Distinguished Graduate Fellowship (to B.J.F.) and an NSF Graduate Research Fellowship (to M.T.V.). R.W.T. is funded by a Wellcome Trust Strategic Award (096919/Z/11/Z), MRC Centre for Neuromuscular Diseases (G0601943), UK NHS Highly Specialised "Rare Mitochondrial Disorders of Adults and Children" Service, and The Lily Foundation. C.L.A. is the recipient of a National Institute for Health Research (NIHR) doctoral fellowship (NIHR-HCS-D12-03-04). H.P. was supported by the German Bundesministerium für Bildung und Forschung (BMBF) through the German Network for mitochondrial disorders (mitoNET, 01GM1113C) and the E-Rare project GENOMIT (01GM1603), the EC FP7-PEOPLE-ITN Mitochondrial European Educational Training Project (GA #317433) and EU Horizon2020 Collaborative Research Project SOUND (633974).

Received: June 30, 2015
Revised: March 25, 2016
Accepted: June 21, 2016
Published: August 4, 2016

REFERENCES

Adam, A.C., Bornhövd, C., Prokisch, H., Neupert, W., and Hell, K. (2006). The Nfs1 interacting protein Isd11 has an essential role in Fe/S cluster biogenesis in mitochondria. EMBO J. *25*, 174–183.

Angerer, H. (2015). Eukaryotic LYR Proteins Interact with Mitochondrial Protein Complexes. Biology (Basel) *4*, 133–150.

Angerer, H., Radermacher, M., Mańkowska, M., Steger, M., Zwicker, K., Heide, H., Wittig, I., Brandt, U., and Zickermann, V. (2014). The LYR protein subunit NB4M/NDUFA6 of mitochondrial complex I anchors an acyl carrier protein and is essential for catalytic activity. Proc. Natl. Acad. Sci. USA *111*, 5207–5212.

Ashraf, S., Gee, H.Y., Woerner, S., Xie, L.X., Vega-Warner, V., Lovric, S., Fang, H., Song, X., Cattran, D.C., Avila-Casado, C., et al. (2013). ADCK4 mutations promote steroid-resistant nephrotic syndrome through CoQ10 biosynthesis disruption. J. Clin. Invest. *123*, 5179–5189.

Atkinson, A., Smith, P., Fox, J.L., Cui, T.-Z., Khalimonchuk, O., and Winge, D.R. (2011). The LYR protein Mzm1 functions in the insertion of the Rieske Fe/S protein in yeast mitochondria. Mol. Cell. Biol. *31*, 3988–3996.

Calvo, S.E., Tucker, E.J., Compton, A.G., Kirby, D.M., Crawford, G., Burtt, N.P., Rivas, M., Guiducci, C., Bruno, D.L., Goldberger, O.A., et al. (2010). High-throughput, pooled sequencing identifies mutations in NUBPL and FOXRED1 in human complex I deficiency. Nat. Genet. *42*, 851–858.

Calvo, S.E., Clauser, K.R., and Mootha, V.K. (2016). MitoCarta2.0: an updated inventory of mammalian mitochondrial proteins. Nucleic Acids Res. *44* (D1), D1251–D1257.

Cox, J., and Mann, M. (2008). MaxQuant enables high peptide identification rates, individualized p.p.b.-range mass accuracies and proteome-wide protein quantification. Nat. Biotechnol. *26*, 1367–1372.

Cox, J., Neuhauser, N., Michalski, A., Scheltema, R.A., Olsen, J.V., and Mann, M. (2011). Andromeda: a peptide search engine integrated into the MaxQuant environment. J. Proteome Res. *10*, 1794–1805.

Cox, J., Hein, M.Y., Luber, C.A., Paron, I., Nagaraj, N., and Mann, M. (2014). Accurate proteome-wide label-free quantification by delayed normalization and maximal peptide ratio extraction, termed MaxLFQ. Mol. Cell. Proteomics *13*, 2513–2526.

Ehses, S., Raschke, I., Mancuso, G., Bernacchia, A., Geimer, S., Tondera, D., Martinou, J.-C., Westermann, B., Rugarli, E.I., and Langer, T. (2009). Regulation of OPA1 processing and mitochondrial fusion by m-AAA protease isoenzymes and OMA1. J. Cell Biol. *187*, 1023–1036.

Fernández-Vizarra, E., and Zeviani, M. (2015). Nuclear gene mutations as the cause of mitochondrial complex III deficiency. Front. Genet. *6*, 134.

Ghezzi, D., Goffrini, P., Uziel, G., Horvath, R., Klopstock, T., Lochmüller, H., D'Adamo, P., Gasparini, P., Strom, T.M., Prokisch, H., et al. (2009). SDHAF1, encoding a LYR complex-II specific assembly factor, is mutated in SDH-defective infantile leukoencephalopathy. Nat. Genet. *41*, 654–656.

Grimsrud, P.A., Carson, J.J., Hebert, A.S., Hubler, S.L., Niemi, N.M., Bailey, D.J., Jochem, A., Stapleton, D.S., Keller, M.P., Westphall, M.S., et al. (2012). A quantitative map of the liver mitochondrial phosphoproteome reveals post-translational control of ketogenesis. Cell Metab. *16*, 672–683.

Guarani, V., Paulo, J., Zhai, B., Huttlin, E.L., Gygi, S.P., and Harper, J.W. (2014). TIMMDC1/C3orf1 functions as a membrane-embedded mitochondrial complex I assembly factor through association with the MCIA complex. Mol. Cell. Biol. *34*, 847–861.

Haack, T.B., Madignier, F., Herzer, M., Lamantea, E., Danhauser, K., Invernizzi, F., Koch, J., Freitag, M., Drost, R., Hillier, I., et al. (2011). Mutation screening of 75 candidate genes in 152 complex I deficiency cases identifies pathogenic variants in 16 genes including NDUFB9. J. Med. Genet. *49*, 83–89.

Haack, T.B., Staufner, C., Köpke, M.G., Straub, B.K., Kölker, S., Thiel, C., Freisinger, P., Baric, I., McKiernan, P.J., Dikow, N., et al. (2015). Biallelic mutations in NBAS cause recurrent acute liver failure with onset in infancy. Am. J. Hum. Genet. *97*, 163–169.

He, C.H., Xie, L.X., Allan, C.M., Tran, U.C., and Clarke, C.F. (2014). Coenzyme Q supplementation or over-expression of the yeast Coq8 putative kinase stabilizes multi-subunit Coq polypeptide complexes in yeast coq null mutants. Biochim. Biophys. Acta *1841*, 630–644.

Hein, M.Y., Hubner, N.C., Poser, I., Cox, J., Nagaraj, N., Toyoda, Y., Gak, I.A., Weisswange, I., Mansfeld, J., Buchholz, F., et al. (2015). A human interactome in three quantitative dimensions organized by stoichiometries and abundances. Cell *163*, 712–723.

Hosp, F., Scheltema, R.A., Eberl, H.C., Kulak, N.A., Keilhauer, E.C., Mayr, K., and Mann, M. (2015). A double-barrel liquid chromatography-tandem mass spectrometry (LC-MS/MS) system to quantify 96 interactomes per day. Mol. Cell. Proteomics *14*, 2030–2041.

Hung, V., Zou, P., Rhee, H.-W., Udeshi, N.D., Cracan, V., Svinkina, T., Carr, S.A., Mootha, V.K., and Ting, A.Y. (2014). Proteomic mapping of the human mitochondrial intermembrane space in live cells via ratiometric APEX tagging. Mol. Cell *55*, 332–341.

Huttlin, E.L., Ting, L., Bruckner, R.J., Gebreab, F., Gygi, M.P., Szpyt, J., Tam, S., Zarraga, G., Colby, G., Baltier, K., et al. (2015). The BioPlex Network: a systematic exploration of the human interactome. Cell *162*, 425–440.

Jäger, S., Cimermancic, P., Gulbahce, N., Johnson, J.R., McGovern, K.E., Clarke, S.C., Shales, M., Mercenne, G., Pache, L., Li, K., et al. (2012). Global landscape of HIV-human protein complexes. Nature *481*, 365–370.

Jain-Ghai, S., Cameron, J.M., Al Maawali, A., Blaser, S., MacKay, N., Robinson, B., and Raiman, J. (2013). Complex II deficiency—a case report and review of the literature. Am. J. Med. Genet. A. *161A*, 285–294.

Keilhauer, E.C., Hein, M.Y., and Mann, M. (2015). Accurate protein complex retrieval by affinity enrichment mass spectrometry (AE-MS) rather than affinity purification mass spectrometry (AP-MS). Mol. Cell. Proteomics *14*, 120–135.

Khadria, A.S., Mueller, B.K., Stefely, J.A., Tan, C.H., Pagliarini, D.J., and Senes, A. (2014). A Gly-zipper motif mediates homodimerization of the

transmembrane domain of the mitochondrial kinase ADCK3. J. Am. Chem. Soc. *136*, 14068–14077.

Kim, J.J., and Miura, R. (2004). Acyl-CoA dehydrogenases and acyl-CoA oxidases. Structural basis for mechanistic similarities and differences. Eur. J. Biochem. *271*, 483–493.

Kirby, D.M., Thorburn, D.R., Turnbull, D.M., and Taylor, R.W. (2007). Biochemical assays of respiratory chain complex activity. Methods Cell Biol. *80*, 93–119.

Koopman, W.J.H., Willems, P.H.G.M., and Smeitink, J.A.M. (2012). Monogenic mitochondrial disorders. N. Engl. J. Med. *366*, 1132–1141.

Lefebvre-Legendre, L., Vaillier, J., Benabdelhak, H., Velours, J., Slonimski, P.P., and di Rago, J.P. (2001). Identification of a nuclear gene (FMC1) required for the assembly/stability of yeast mitochondrial F(1)-ATPase in heat stress conditions. J. Biol. Chem. *276*, 6789–6796.

Lohman, D.C., Forouhar, F., Beebe, E.T., Stefely, M.S., Minogue, C.E., Ulbrich, A., Stefely, J.A., Sukumar, S., Luna-Sánchez, M., Jochem, A., et al. (2014). Mitochondrial COQ9 is a lipid-binding protein that associates with COQ7 to enable coenzyme Q biosynthesis. Proc. Natl. Acad. Sci. USA *111*, E4697–E4705.

Makino, S.-i., Beebe, E.T., Markley, J.L., and Fox, B.G. (2013). Cell-Free Protein Synthesis for Functional and Structural Studies (Totowa, N.J.: Humana Press), pp. 161–178.

Marbois, B., Gin, P., Faull, K.F., Poon, W.W., Lee, P.T., Strahan, J., Shepherd, J.N., and Clarke, C.F. (2005). Coq3 and Coq4 define a polypeptide complex in yeast mitochondria for the biosynthesis of coenzyme Q. J. Biol. Chem. *280*, 20231–20238.

Matsunaga, T., Endo, S., Maeda, S., Ishikura, S., Tajima, K., Tanaka, N., Nakamura, K.T., Imamura, Y., and Hara, A. (2008). Characterization of human DHRS4: an inducible short-chain dehydrogenase/reductase enzyme with 3beta-hydroxysteroid dehydrogenase activity. Arch. Biochem. Biophys. *477*, 339–347.

Modjtahedi, N., Tokatlidis, K., Dessen, P., and Kroemer, G. (2016). Mitochondrial proteins containing coiled-coil-helix-coiled-coil-helix (CHCH) domains in health and disease. Trends Biochem. Sci. *41*, 245–260.

Nguyen, T.P.T., Casarin, A., Desbats, M.A., Doimo, M., Trevisson, E., Santos-Ocaña, C., Navas, P., Clarke, C.F., and Salviati, L. (2014). Molecular characterization of the human COQ5 C-methyltransferase in coenzyme Q10 biosynthesis. Biochim. Biophys. Acta *1841*, 1628–1638.

Nunnari, J., and Suomalainen, A. (2012). Mitochondria: in sickness and in health. Cell *148*, 1145–1159.

Pagliarini, D.J., and Rutter, J. (2013). Hallmarks of a new era in mitochondrial biochemistry. Genes Dev. *27*, 2615–2627.

Pagliarini, D.J., Calvo, S.E., Chang, B., Sheth, S.A., Vafai, S.B., Ong, S.E., Walford, G.A., Sugiana, C., Boneh, A., Chen, W.K., et al. (2008). A mitochondrial protein compendium elucidates complex I disease biology. Cell *134*, 112–123.

Persson, B., and Kallberg, Y. (2013). Classification and nomenclature of the superfamily of short-chain dehydrogenases/reductases (SDRs). Chem. Biol. Interact. *202*, 111–115.

Rhee, H.-W., Zou, P., Udeshi, N.D., Martell, J.D., Mootha, V.K., Carr, S.A., and Ting, A.Y. (2013). Proteomic mapping of mitochondria in living cells via spatially restricted enzymatic tagging. Science *339*, 1328–1331.

Roberts, D.L., Frerman, F.E., and Kim, J.J. (1996). Three-dimensional structure of human electron transfer flavoprotein to 2.1-A resolution. Proc. Natl. Acad. Sci. USA *93*, 14355–14360.

Rodrigues, J.V., and Gomes, C.M. (2012). Mechanism of superoxide and hydrogen peroxide generation by human electron-transfer flavoprotein and pathological variants. Free Radic. Biol. Med. *53*, 12–19.

Saada, A., Vogel, R.O., Hoefs, S.J., van den Brand, M.A., Wessels, H.J., Willems, P.H., Venselaar, H., Shaag, A., Barghuti, F., Reish, O., et al. (2009). Mutations in NDUFAF3 (C3ORF60), encoding an NDUFAF4 (C6ORF66)-interacting complex I assembly protein, cause fatal neonatal mitochondrial disease. Am. J. Hum. Genet. *84*, 718–727.

Saada, A., Edvardson, S., Shaag, A., Chung, W.K., Segel, R., Miller, C., Jalas, C., and Elpeleg, O. (2012). Combined OXPHOS complex I and IV defect, due to mutated complex I assembly factor C20ORF7. J. Inherit. Metab. Dis. *35*, 125–131.

Sahni, N., Yi, S., Taipale, M., Fuxman Bass, J.I., Coulombe-Huntington, J., Yang, F., Peng, J., Weile, J., Karras, G.I., Wang, Y., et al. (2015). Widespread macromolecular interaction perturbations in human genetic disorders. Cell *161*, 647–660.

Sánchez, E., Lobo, T., Fox, J.L., Zeviani, M., Winge, D.R., and Fernández-Vizarra, E. (2013). LYRM7/MZM1L is a UQCRFS1 chaperone involved in the last steps of mitochondrial Complex III assembly in human cells. Biochim. Biophys. Acta *1827*, 285–293.

Schiff, M., Froissart, R., Olsen, R.K., Acquaviva, C., and Vianey-Saban, C. (2006). Electron transfer flavoprotein deficiency: functional and molecular aspects. Mol. Genet. Metab. *88*, 153–158.

Seiler, C.Y., Park, J.G., Sharma, A., Hunter, P., Surapaneni, P., Sedillo, C., Field, J., Algar, R., Price, A., Steel, J., et al. (2014). DNASU plasmid and PSI:Biology-Materials repositories: resources to accelerate biological research. Nucleic Acids Res. *42*, D1253–D1260.

Shan, Y., Napoli, E., and Cortopassi, G. (2007). Mitochondrial frataxin interacts with ISD11 of the NFS1/ISCU complex and multiple mitochondrial chaperones. Hum. Mol. Genet. *16*, 929–941.

Sowa, M.E., Bennett, E.J., Gygi, S.P., and Harper, J.W. (2009). Defining the human deubiquitinating enzyme interaction landscape. Cell *138*, 389–403.

Stefely, J.A., Reidenbach, A.G., Ulbrich, A., Oruganty, K., Floyd, B.J., Jochem, A., Saunders, J.M., Johnson, I.E., Minogue, C.E., Wrobel, R.L., et al. (2015). Mitochondrial ADCK3 employs an atypical protein kinase-like fold to enable coenzyme Q biosynthesis. Mol. Cell *57*, 83–94.

Stefely, J.A., Licitra, F., Laredj, L., Reidenbach, A.G., Kemmerer, Z.A., Grangeray, A., Jaeg-Ehret, T., Minogue, C.E., Ulbrich, A., Hutchins, P.D., et al. (2016). Cerebellar ataxia and coenzyme Q deficiency through loss of unorthodox kinase activity. Mol. Cell *63*, Published online August 4, 2016. http://dx.doi.org/10.1016/j.molcel.2016.06.030.

Still, A.J., Floyd, B.J., Hebert, A.S., Bingman, C.A., Carson, J.J., Gunderson, D.R., Dolan, B.K., Grimsrud, P.A., Dittenhafer-Reed, K.E., Stapleton, D.S., et al. (2013). Quantification of mitochondrial acetylation dynamics highlights prominent sites of metabolic regulation. J. Biol. Chem. *288*, 26209–26219.

Sugiana, C., Pagliarini, D.J., McKenzie, M., Kirby, D.M., Salemi, R., Abu-Amero, K.K., Dahl, H.H., Hutchison, W.M., Vascotto, K.A., Smith, S.M., et al. (2008). Mutation of C20orf7 disrupts complex I assembly and causes lethal neonatal mitochondrial disease. Am. J. Hum. Genet. *83*, 468–478.

Vockley, J., and Whiteman, D.A. (2002). Defects of mitochondrial beta-oxidation: a growing group of disorders. Neuromuscul. Disord. *12*, 235–246.